Materials Science and Engineering A 371 (2004) 91–102

MATERIALS SCIENCE & ENGINEERING A

www.elsevier.com/locate/msea

Microstructural evolution during remelting of laser surface alloyed hyper-monotectic Al–Bi alloy

Gandham Phanikumar [a], Pradip Dutta [b], Rolf Galun [c], Kamanio Chattopadhyay [a,*]

[a] *Department of Metallurgy, Indian Institute of Science, Bangalore 560012, India*
[b] *Department of Mechanical Engineering, Indian Institute of Science, Bangalore 560012, India*
[c] *Institut für Werkstoffkunde und Werkstofftechnik, Technische Universität Clausthal, Clausthal-Zellerfeld, Germany*

Received 18 June 2003; received in revised form 8 September 2003

Abstract

The present investigation explores the possibility of synthesizing a two-phase microstructure consisting of a fine dispersion of bismuth particles in an aluminium matrix using the laser surface alloying technique. The possibility of controlling the size distribution of bismuth particles by subsequent remelting is also investigated. The microstructural analysis of the surface alloyed samples shows that the average size of the bismuth particles reduces with increase in laser scan speed. In order to understand the factors that determine the nature of the size distribution of the particles, a detailed model is developed. The model incorporates heat and fluid flow induced by the laser to arrive at the evolution of the temperature and velocity of the melt in three dimensions. Using these as inputs, a kinetic analysis of the nucleation, growth and coarsening induced by collision-controlled coalescence of the bismuth particles from the melt is carried out. Comparison with the experiments indicates that coalescence due to convection plays an important role in the evolution of the size distribution of bismuth particles.

Keywords: Al–Bi; Hyper-monotectic; Laser surface alloying; Dispersion; Microstructure evolution; Immiscible

1. Introduction

Aluminium alloys dispersed with lead, bismuth and tin show promising applications in the tribology of automotive components [1]. Such dispersions of low melting temperature elements exhibit low hardness and flow easily under sliding conditions, resulting in favourable tribological behaviour. The binary phase diagram of aluminium–bismuth [2] contains a monotectic reaction followed by a domain of liquid immiscibility. Thus, a hyper-monotectic alloy liquid is separated into globules of bismuth dispersed in a matrix of aluminium upon cooling from a temperature above the critical line bounding the immiscible domain. The conventional casting route to produce alloys of Al–X (X: Pb/Bi/Sn) leads to a coarse microstructure with segregation and sedimentation of the heavier phase, [3,4] which may be avoided in the presence of vigorous convection. Techniques such as magnetohydrodynamic processing take advantage of the convection to produce a uniform dispersion of soft phase in a metallic matrix [5,6]. In this work, laser surface alloying followed by laser remelting is conducted to produce uniform dispersions of a soft phase on the surface of a desired material. Pure aluminium is chosen as the substrate and bismuth as the soft phase. A numerical model is developed to understand the factors that govern the bismuth particle size distribution in the alloyed layer as a function of process parameters. The modelling results are compared with the experiments.

2. Experimental study

A schematic of the experimental setup for laser surface alloying and remelting is shown in Fig. 1. In addition to the laser, the setup consists of a substrate holder mounted on a computer controlled X–Y stage and a powder feeding system. The detailed experimental conditions are listed in Table 1. Elemental powders (40–70 μm) of commercial purity aluminium and bismuth are blended (in 10:1, w/w ratio) and fed into the laser melt pool using the powder feeder. Both the laser and powder feeder remain stationary during

* Corresponding author. Tel.: +91-80-22932678; fax: +91-80-3600683.
E-mail address: kamanio@metalrg.iisc.ernet.in (K. Chattopadhyay).

0921-5093/$ – see front matter © 2003 Elsevier B.V. All rights reserved.
doi:10.1016/j.msea.2003.09.071

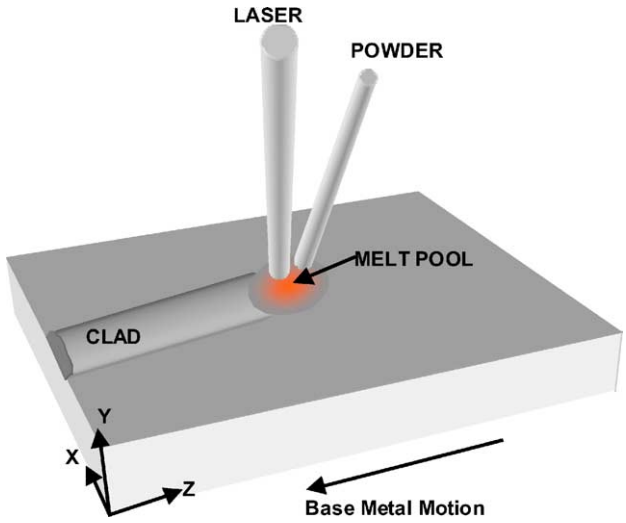

Fig. 1. Schematic of the laser cladding process.

the experiment while the substrate is moved at a predetermined speed to produce the alloyed track on the substrate. The substrate is kept 30 mm above the focal point of the laser to obtain a large beam diameter of 3 mm. This results in a broad distribution of intensity that does not lead to vaporization of the substrate material. The alloyed layers were subsequently used for surface remelting at higher speeds to simulate higher solidification rates. The remelting experiments followed the same procedure except that no powder is fed during the process. The present study is restricted to single-pass alloying in order to make a meaningful study on the effect of processing conditions on the bismuth particle size distribution.

Initial experiments of alloying using laser powers of 3–4 kW produced alloyed layers with poor adherence to the substrate and lack of uniformity along the length of the alloyed track. To obtain a smooth and porosity-free alloyed layer with uniform distribution of bismuth particles in aluminium matrix, a high laser power of 8.5 kW and a scan rate of 5 mm/s was found to be optimum and used for this study. When the laser power is increased, peak temperatures are much higher than the temperature of liquid miscibility gap. Thus, the solidification takes place from the melt layer with bismuth completely in the solution. Under such a scenario, phase separation in the melt competes with the solidification yielding a dispersed microstructure at higher growth rate.

3. Experimental results

X-ray diffraction patterns of the surface alloyed layers as well as the layers remelted subsequently showed only the elemental peaks of aluminium and bismuth. Scanning electron microscopy (SEM) indicates the presence of dispersed particles in the aluminium matrix. The average composition of the alloyed layer using the EDS analyzer estimated to be 0.78 at.% Bi. This value is less than the composition of the powder used (1.414 at.% Bi) because of dilution by the substrate.

A typical microstructure of a surface alloyed track remelted at a scan rate of 5 mm/s is shown in Fig. 2. The transverse section shown in Fig. 2a clearly reveals the original surface alloyed layer and the remelted layer. Although the processing conditions are identical, the remelted depth is less than the alloyed depth due to enhanced absorption of the laser radiation by the powder in flight during alloying. The increase in laser scan rate reduces the depth of the remelted layer further. Both the alloyed and remelted regions exhibit directional growth of aluminium grains from the substrate into the alloyed melt. This is revealed in the longitudinal section shown in Fig. 2b. Bismuth particles were imaged using a back scattered electron detector in the scanning electron microscope (BSE). Fig. 2c shows a typical BSE micrograph of the cross-sections of a remelted region revealing a fine dispersion of the bismuth particles (light) in the aluminium matrix (dark). The microstructure reveals distribuition of fine submicron particles. However, few bismuth particles are much larger than the average. The microstructure is fairly uniform across the remelted layers.

For more quantitative information, the size distribution analysis has been carried out on the remelted tracks (regions covering 1 mm from the top). A series of microstructures are taken in both transverse and longitudinal sections to determine the size distribution of the particles using an image

Table 1
Experimental parameters

Laser: Rofin Sinar R10000, cw CO_2
Peak laser power: 10 KW
Laser beam diameter on substrate at 30 mm defocus: 3 mm
Protective gas shroud: Ar + 30% (v/v) He
Powder feeder: Metko
Feeder gas: Ar + 30% (v/v) He
Gas flow rate is adjusted to yield a feed rate of 1.2 g/s
Powder composition: Al + 10 wt.% Bi (Al + 1.414 at.% Bi)

Laser scan speeds (mm/s)	5 (surface alloying)	5 (remelting)	13 (remelting)	20 (remelting)
Bismuth particle size average (μm)	0.73	0.80	0.51	0.44

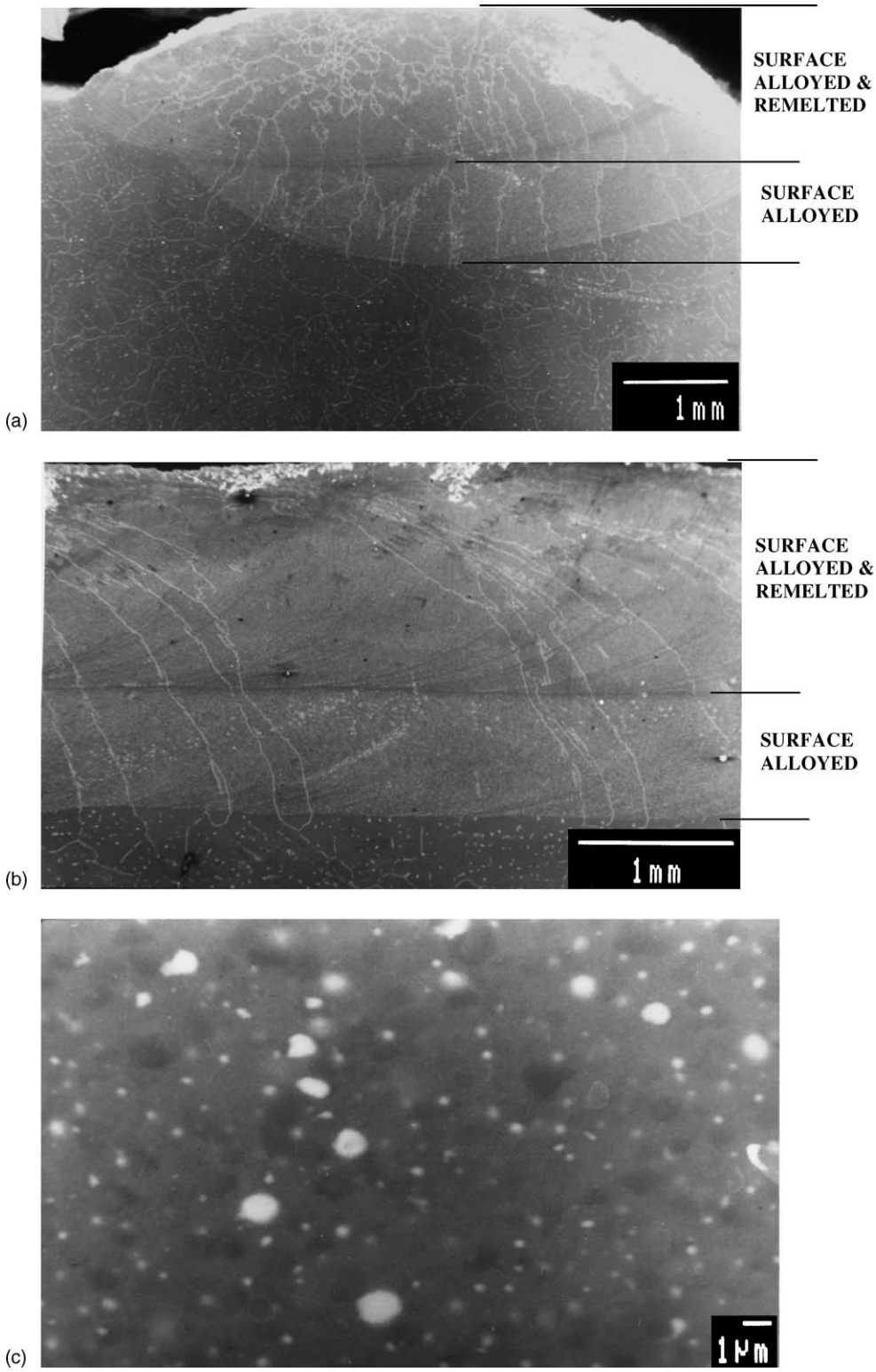

Fig. 2. (a) Transverse section and (b) longitudinal section of surface alloyed and remelted regions for the laser scan speed of 5 mm/s. (c) Distribution of bismuth particles within the remelted region near the top.

analysis software. Since the particles are nearly rounded in shape, the Feret diameter (diameter of a circle of the same area as that of the particle) is used as the representative parameter for determining the diameters of the particles. The distributions of particle sizes plotted for the surface alloyed and remelted alloys are shown in Fig. 3. Average sizes are given in Table 1. As can be noted, the average particle size decreases with increasing laser scan speed. However, the

distribution shows a log-normal nature, with a considerable number of particles much larger than the average size. In the section that follows, a computational model is discussed to determine the factors that govern the size distribution of surface remelted Al–Bi hyper-monotectic alloy.

4. Computational study

The model assumes that the dispersed second phase Bi particles evolve in the melt and the solidification of the matrix does not alter the sizes of the particles. Hence, the process of microstructure evolution during the laser surface alloying could be visualized in two stages. At the macro level, the laser melting with the consequent heat transfer and fluid flow dictates the size and shape of the melt zone. The thermal history of the various locations in the remelted region is given by the solution of the governing transport equations used for modelling the laser melting problem. At the micro level, the microstructure is determined by the nucleation, growth, coarsening and coalescence of the dispersed liquid phase in the melt pool during cooling. Time scale of these processes is determined by the thermal history. Thus, one has an option of modelling the

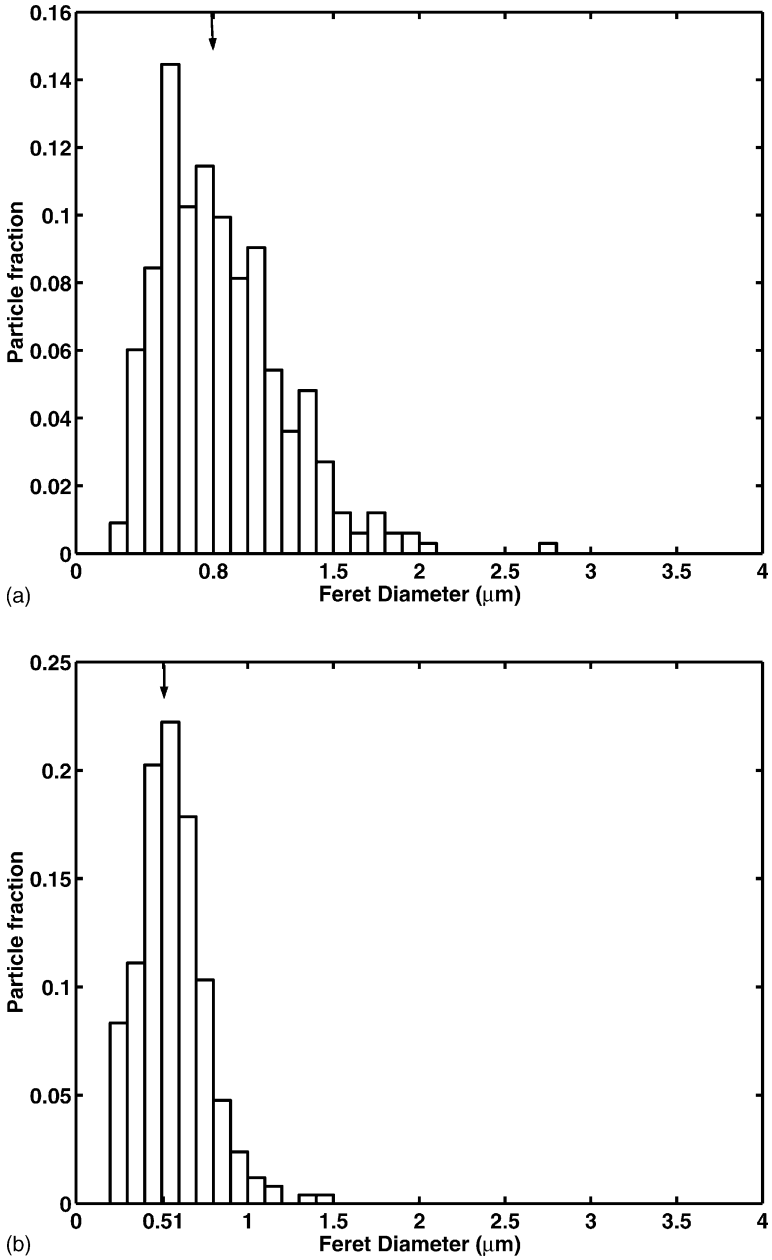

Fig. 3. Apparent distribution of bismuth particle size (Feret diameter) of surface alloyed and remelted layers at (a) 5 mm/s (b) 13 mm/s and (c) 20 mm/s. Average sizes are indicated by the arrows.

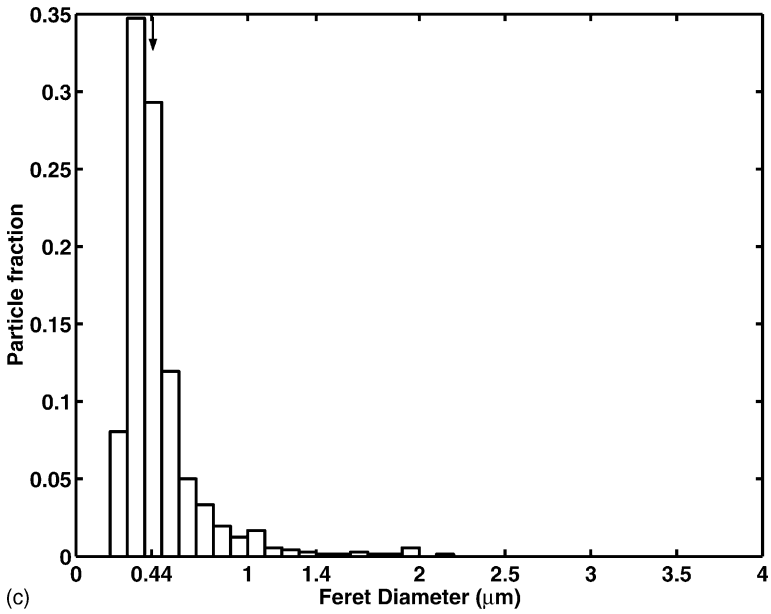

Fig. 3. (*Continued*).

problem in two stages to arrive at the final picture of the microstructure in terms of size distribution of the dispersed phase. A flow chart of the computational model is shown in Fig. 4.

4.1. Laser melting

A three dimensional transient model developed by the authors for laser processing [7,8] has been used for modelling laser remelting. The Al–Bi alloy exists as a dilute solution and is assumed to be well mixed at the macro level. The final shape of the melt pool, temperature gradients in the liquid, and thus the cooling rate at any location in the pool are strongly affected by convection. In the present case, convection in the liquid melt pool is predominantly due to surface-tension driven (Marangoni) convection on the free surface rather than buoyancy forces in the bulk of the melt pool [7]. The Marangoni forces are incorporated as boundary conditions for the velocities on the free surface. The formulation uses the well-established enthalpy-porosity model, the details of which are given elsewhere [7,8]. The governing equations are discretized and solved using a control volume method according to the SIMPLER algorithm [9]. The computational parameters used are listed in Table 2.

Table 2
Parameters used in the laser melting program

Laser power, q (W)	8500
Coupling efficiency, η	0.20
Radius of laser on sample surface, r_q (mm)	1.5
Dimensions of computational domain (mm^3)	30 × 10 × 30
Number of grids	64 × 48 × 64

The value of laser efficiency is initially adjusted such that the pool shape matches with that of the experiment for one of the remelting speeds. The same value of efficiency is observed to reproduce the experimentally observed pool shape for the remaining scanning speeds and thus is kept constant.

Fig. 5 shows the computed temperature contours and velocity profile in the top view and longitudinal section of the remelted region for a laser scan speed of 5 mm/s. The computed shape of the solidification front matches the trace left by the moving solidification front observable in Fig. 2b. Due to the negative temperature coefficient of surface tension in aluminium, the liquid flows radially outward from the laser centre on the top surface. The maximum velocity is at the top of the pool near the solid-liquid interface and is about 2 m/s in magnitude. The cooling rate obtained from the thermal history within any given temperature interval form the input for the nucleation and growth calculations discussed in the next section. A typical example of heating and cooling curve of a point in the melt pool is shown in Fig 5c.

4.2. Nucleation and growth

Nucleation of the second phase in the liquid immiscible systems outside the spinodal regime can be quantitatively described using homogeneous nucleation theory as shown by Granasy and Ratke [10] and Christian [11]. The homogeneous nucleation rate for phase separation is given by $I = I_0 \exp(-(16\pi/3k_BT)(\sigma^3/\Delta G_v^2))$, where ΔG_v is the volume free energy, σ is the surface tension between the liquids of Al and Bi.

The free energy of the Al–Bi system (in J mol^{-1}) in the temperature range of immiscibility (930–1310 K) is given by an expression below using subregular solution model [12].

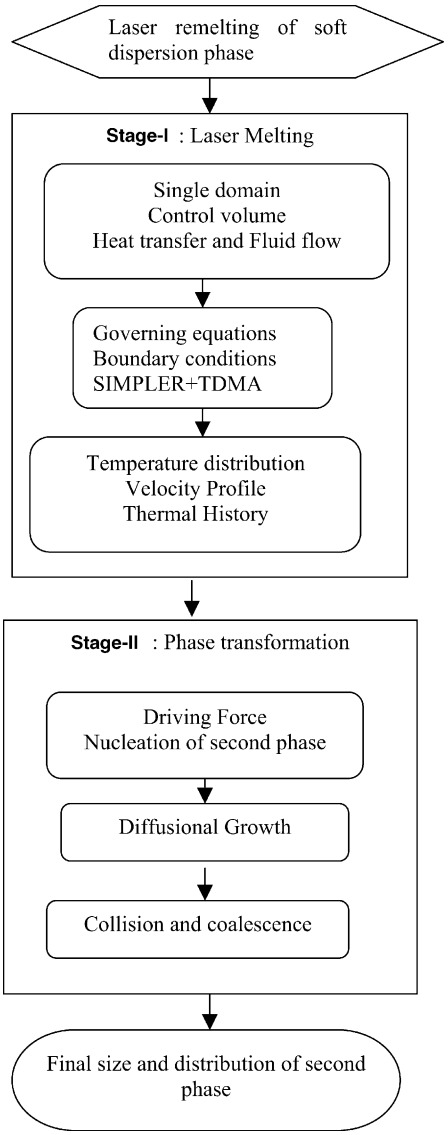

Fig. 4. Flow chart of the modelling scheme.

x_1 and x_2 are the compositions of aluminium and bismuth, respectively.

$$\Delta G = (24649.18 - 3.0497T)x_1x_2 + (13282.64 - 5.92753T)x_1x_2(x_1 - x_2) + (18519.75 - 12.33873T)x_1x_2(x_1 - x_2)^2 + (6959.30 - 2.24613T)x_1x_2(x_1 - x_2)^3 + \mathrm{RT}(x_1 \log x_1 + x_2 \log x_2)$$

The driving force for the nucleation of the second phase in alloy melts (ΔG_v) was obtained from the free energy using the method proposed by Thompson and Spaepen [13]. In order to obtain the nucleation rate, it is necessary to know surface energy (σ) between the two separating liquids at different temperatures. The surface energy of a critical system such as the immiscible Al–Bi liquid is described by a power law scaling relation [14]. The critical values for the case of Al–Bi system are available in the literature [15].

Table 3
Parameters used in the nucleation and growth calculations

Surface tension, σ (Nm^{-1})	$0.2854(1.0 - T/1310)^{1.26}$
Average jump distance, λ (m)	3.64×10^{-10}
Atomic volume of Al, Ω(m^3)	1.2249×10^{-29}
Atomic volume of Bi, Ω (m^3)	2.5252×10^{-29}
Viscosity of Al, μ ($\mathrm{Nm}^{-2}\,\mathrm{s}$)	$0.1492 \times 10^{-3} \exp(16500/8.314T)$
Viscosity of Bi, μ ($\mathrm{Nm}^{-2}\,\mathrm{s}$)	$0.4458 \times 10^{-3} \exp(6450/8.314T)$
Molar weight of Al (kg)	0.02698
Molar weight of Bi (kg)	0.20898
Density of Al ($\mathrm{kg\,m}^{-3}$)	2700
Density of Bi ($\mathrm{kg\,m}^{-3}$)	9550

The pre-exponential factor I_0, evaluated using the classical expression for nucleation rate [16], is a function of composition and temperature and is of the order of $1 \times 10^{-30}\,\mathrm{m}^{-3}\,\mathrm{s}^{-1}$. The parameters used for the calculations are listed in Table 3.

The steady state nucleation rates are calculated as a function of temperature and composition. The calculations are carried out up to a composition of 0.962 at.% Bi. The contours of the same are shown in Fig. 6. It can be observed that the nucleation rate increases exponentially as the temperature decreases. At lower compositions, the liquidus temperature is lower. Therefore, the undercooling for phase separation is smaller and as a consequence the nucleation rate is also lower. Thus, at a given temperature, the nucleation rate is lower at lower compositions of bismuth in the liquid.

Growth of Bi particles can be modeled using the diffusion controlled growth law [17]. Furthermore, the size of Bi particles can be influenced by the surface-energy driven coarsening process. It is possible to estimate the relative importance of the two processes. Assuming that the coarsening process follows LSW kinetics [18,19], the transport constant K_{LSW} [20] is estimated as $K_{\mathrm{LSW}} = (8\sigma\Omega C_0 D)/(9k_{\mathrm{B}}T\,\Delta C)$, where C_0 is the concentration of the decomposing liquid, Ω the atomic volume, T the temperature, k_{B} the Boltzmann constant, ΔC the composition difference between the matrix and the particle and D is diffusivity. At 1030 K, the estimated value of K_{LSW} is $4 \times 10^{-19}\,\mathrm{m}^{-3}\,\mathrm{s}^{-1}$ and diffusivity is $4.7 \times 10^{-9}\,\mathrm{m}^{-3}\,\mathrm{s}^{-1}$. The typical time interval involved at each temperature for the imposed cooling condition is of the order of 1 ms. The increase in diameter of bismuth particle due to diffusional growth for the time interval involved (~1 ms) leads to a size almost two orders of magnitude larger than that estimated for the coarsening process. Thus, the contribution from LSW coarsening for the increase in particle size can be ignored. In the numerical scheme of calculation, only the diffusional growth of nucleated particles is considered till the supersaturation is exhausted.

The temperature at which nucleation and growth of bismuth particles takes place decreases continuously at a rate given by the cooling rate. Thus, to obtain the number of nuclei and the final size distribution of the bismuth particles, nucleation rate and increase in particle size by diffusional

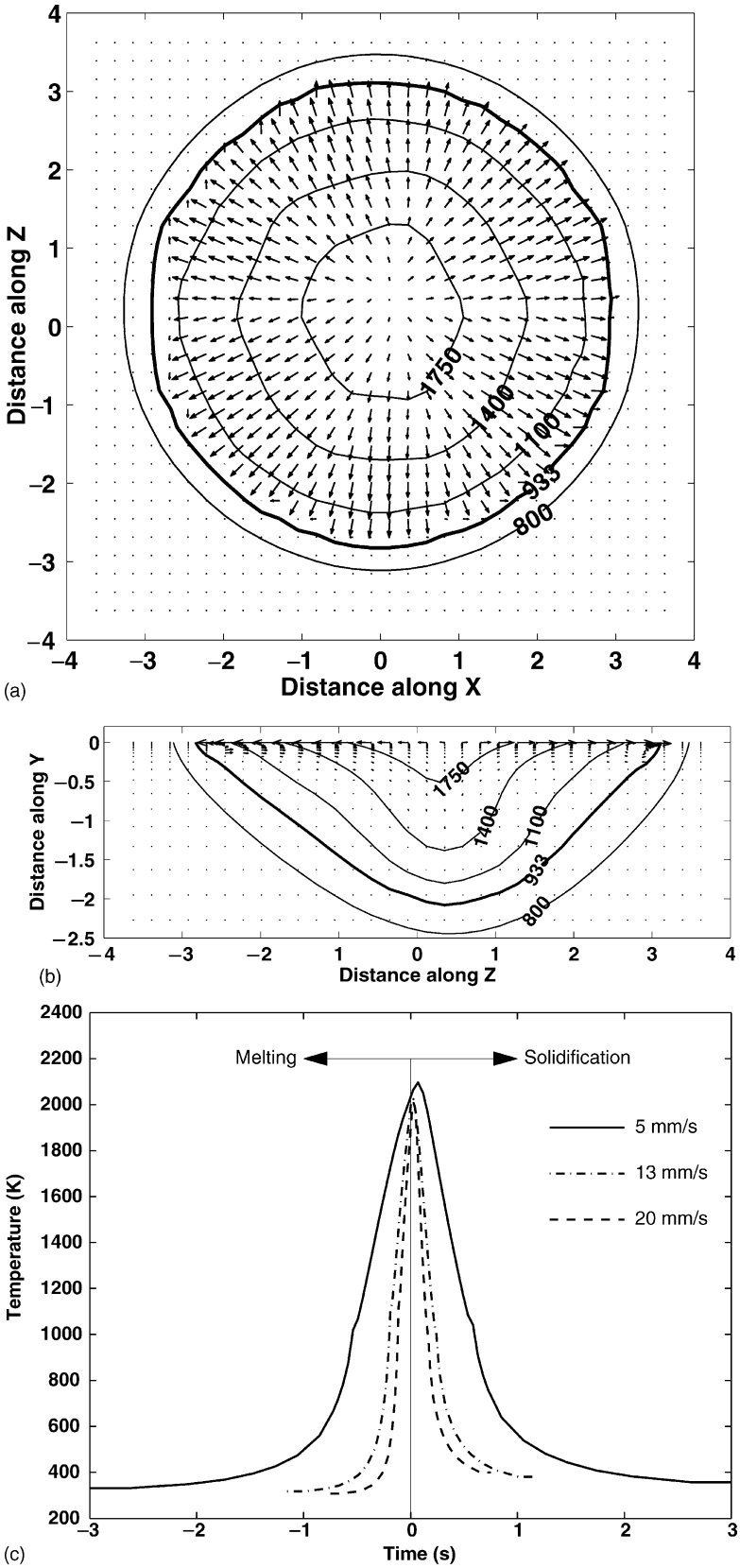

Fig. 5. Temperature contours and velocity profiles in the laser remelted region in (a) top view and (b) longitudinal section for scanning speed of 5 mm/s. The bold contour shows the extent of melting. The contour labels shown are in degrees K, the axes are in mm. (c) Thermal history of a point near the top of the remelted region.

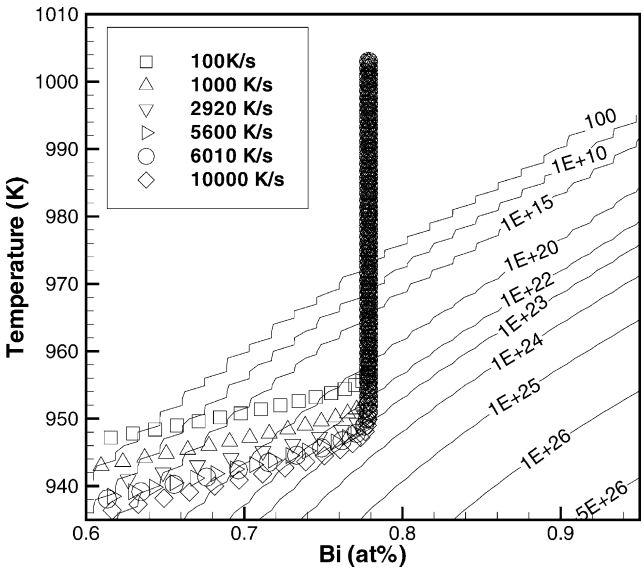

Fig. 6. Temperature-composition path taken by a control volume during phase separation. The contours show steady state nucleation rate.

growth should be calculated taking into account the solute depletion in the melt. The calculations are done for a unit volume in which the mass of bismuth is balanced after every time step. The diffusional growth of particles accumulated up to the time step is calculated by taking their radii and the composition of remaining liquid into account. The composition of bismuth in the control volume decreases during the process and calculations are stopped once the supersaturation is exhausted.

4.3. Size distribution

Fig. 7a shows the size distribution of bismuth particles after phase separation of a liquid at a cooling rate of 6000 K/s for different initial compositions of liquid. The size distribution is broader and the total number of nuclei decreases as the initial composition of bismuth reduces. This is understandable since at lower compositions of bismuth, the steady state nucleation is lower, leading to an increase in the size of the particles before the supersaturation is exhausted. However, the size distribution does not seem to be a strong function of composition.

At different speeds for laser remelting, the dominant parameter that controls the size distribution is the cooling rate. The size distribution of bismuth particles after nucleation and diffusional growth at three different cooling rates: 10^2, 10^3 and 10^4 K/s, is shown in Fig. 7b. The number of nuclei is larger for higher cooling rate and, accordingly, the average size of the particles is smaller. The development of the distribution at different cooling rates can be understood by observing the path taken by a control volume in the temperature-composition map. Fig. 6 shows such a path for different cooling rates superimposed on the contours of nucleation rates as a function of temperature and composition.

At higher cooling rates, the residence time for the melt at each temperature is small. Therefore, the melt undercools to a large extent before significant nucleation takes place. This happens at lower temperature, where the nucleation rate is high. The appearance of particles under this scenario is dominated by the nucleation. Calculations suggest that under this condition, the growth has only a minor influence on the distribution of the particle size of the dispersed phase.

At lower cooling rates, the control volume spends more time in a given temperature range than the case of higher cooling rates. Thus, time is available for the particles that have nucleated at the given temperature intervals and above to grow. The concentration of bismuth, therefore, decreases at relatively higher temperature during cooling and exhaustion of supersaturation occurs at higher temperatures. This scenario at lower cooling rates yields larger particle sizes. It can be noted that the calculated size distribution at this stage is symmetric in shape. This is in contrast to the observed size distributions that are not symmetric and have a significant number of particles at larger size.

4.4. Collision

The nucleation and growth of the bismuth particles take place in a liquid pool that undergoes vigorous convection driven by Marangoni forces. Thus, one expects that coalescence due to the collision of particles will occur during the process. Coalescence can also occur due to sedimentation process driven by gravity. However, it is negligible as the velocities for convection in a laser melt pool are large (of the order of 1 m/s) and thus, significantly higher than the Stokes velocities (of the order of 1 mm/s). Coagulation and coalescence of particles under motion is well studied. A review by Drake [21] provides a comprehensive analysis of models in use for processes involving aerosols and colloids. However, coalescence of particles during solidification is not well understood [16]. The existing models involve collision frequency as a function of velocity of the particles. This term is nearly impossible to evaluate for laser melting for which the velocity profile is solved numerically. The velocity of the fluid varies as a function of position, time, and the process conditions. Considering the above issues, the method outlined below is used to take coalescence into account. The following assumptions are made:

- Particles move along with the liquid and drag is negligible. Collision takes place due to finite sizes of the particles.
- The volume fraction of particles (<2%) is small enough that they do not affect the liquid flow field.
- Particles that have undergone diffusional growth are considered for coalescence during which they only collide and coalesce but do not grow. Growth and coalescence are thus treated as discrete steps in the process.

The velocity profile ahead of the solidification front in the longitudinal section is shown in Fig. 8a. The temperature

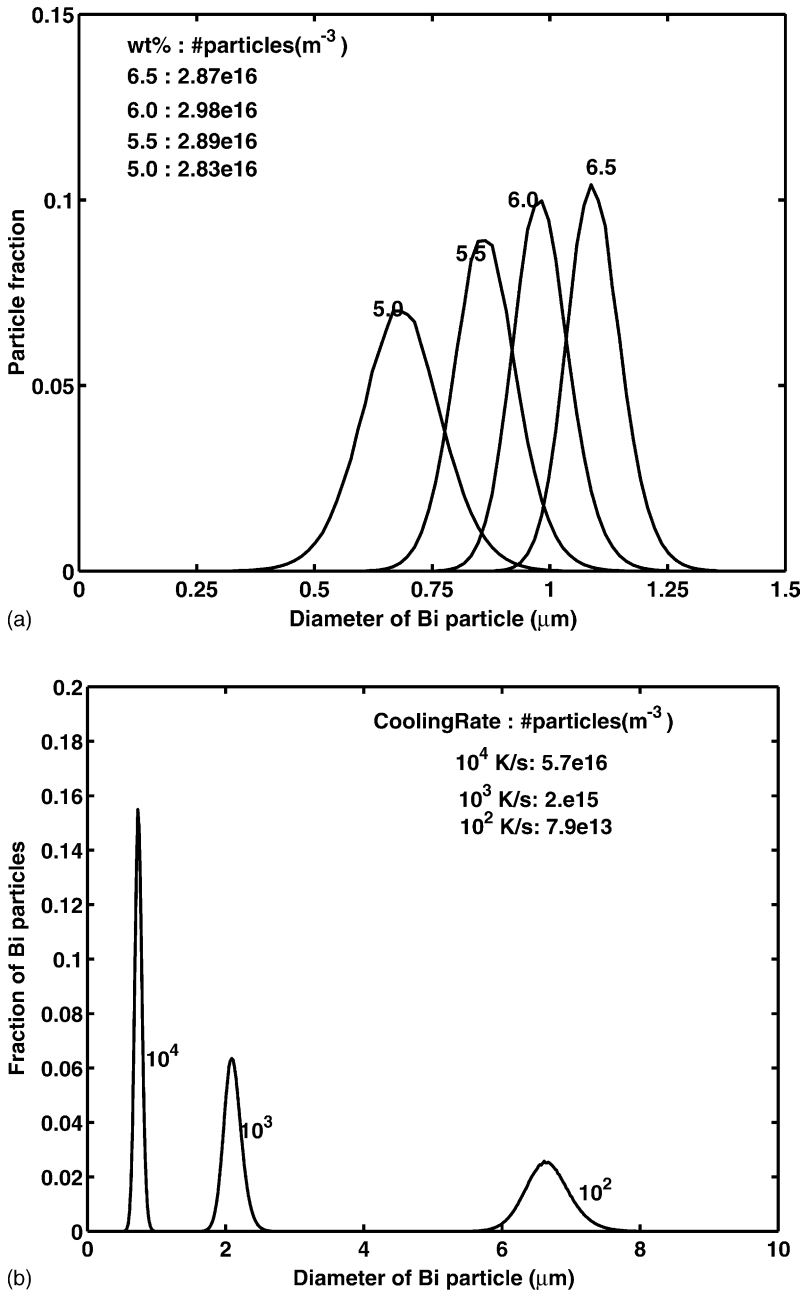

Fig. 7. Size distribution of bismuth particles after nucleation and simultaneous diffusional growth evaluated till exhaustion of supersaturation, as a function of change in (a) composition of bismuth in liquid, (b) cooling rate. The maximum number of nuclei used to normalise the plots are shown in the legend.

contours shown are in degrees K, and correspond to the range within which phase separation takes place for the composition of the alloy under study. The box shown at the right top of the a control volume chosen to study the collision of particles. The time scale shown in Fig. 8b is the total time spent by the control volume within the temperature range of phase separation. During this interval, Δt_1 is the effective time interval when the particles nucleate and grow till supersaturation is exhausted. A number of particles are introduced in a control volume such that the number of particles per unit volume corresponds to the number of nuclei calculated for exhaustion of supersaturation, as detailed in the previous section. The particles are introduced with their sizes corresponding to the distribution after nucleation and growth. The locations of the particles are chosen by a random number generation program. The particles are then tracked in a Lagrangian frame of reference by integrating the fluid velocities at the respective locations using a fourth order Runge–Kutta method. Fluid velocity at non-grid locations is interpolated using a trilinear scheme. Two particles are coalesced and the size of the first particle is increased due to volume conservation when they come in contact

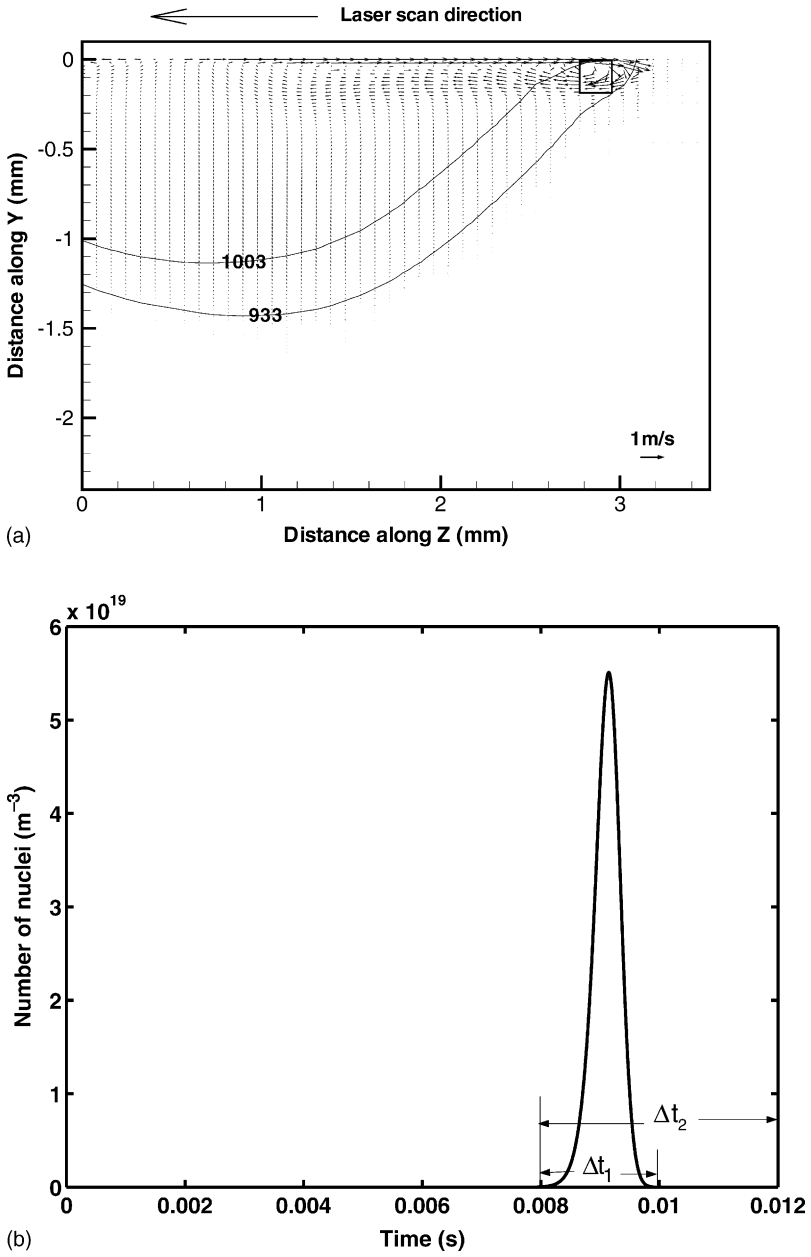

Fig. 8. (a) Velocity profile shown on the solidification front within the temperature range for phase separation. The laser remelting speed used is 20 mm/s. (b) Number of nuclei precipitating out of Al–Bi alloy liquid during the time interval of phase separation. Δt_1 is the time interval chosen to introduce particles into the control volume. And Δt_2 is the time interval for collision.

with each other. The coalescence by collision occurs during a time interval Δt_2 spent by the control volume in the temperature range below which the aluminium matrix solidifies (Fig. 8b). Particle size distribution after coalescence is estimated keeping the total mass of particles in a control volume constant at every time step.

Fig. 9 shows the particle size distributions before and after collision. The size distribution without collision is narrow and nearly symmetric about the mean size. Collision led to an increase in average particle size. The total number of particles decreases during the coalescence. The larger particles have more probability of collision due to size effect and thus the size distribution develops a tail towards the higher size.

5. Comparison with the experiments

The experimentally observed size distribution is compared with the one numerically estimated. A comparison of Fig. 3 with Fig. 9 brings out following conclusion. The nature of the experimentally observed distribution curve is reproduced well in our computational scheme only when the effect of collision due to the large surface tension

driven fluid flow is included. The process of nucleation and growth alone cannot explain the observed size distribution. The computation overestimates the average size of bismuth particles while reproducing the nature of distribution. The quantitative matching with experiments is subject to the accuracy of the input parameters as well as the assumptions in modeling the various physical processes. In our study, the surface tension between the liquids of aluminium and bismuth is taken to be 60 mN/m at monotectic temperature [15]. Recent work by Hoyer et al. [22] report the same to be 66 mN/m. Nucleation rate is a sensitive function of surface tension and increases with decrease in surface tension [7]. Diffusivity in immiscible systems is not easily available and is also estimated from the viscosity. The discrepancy between computation and experiments may be explained partly by the uncertainty in the input parameters and partly by the assumptions in the laser melting problem. Quantitatively, the match between the computed and experimental size distribution is excellent only for the samples processed at the higher scan speed of 20 mm/s. At the lower laser scan speed, the observed distributions of sizes are broader compared to that obtained through computation. The results

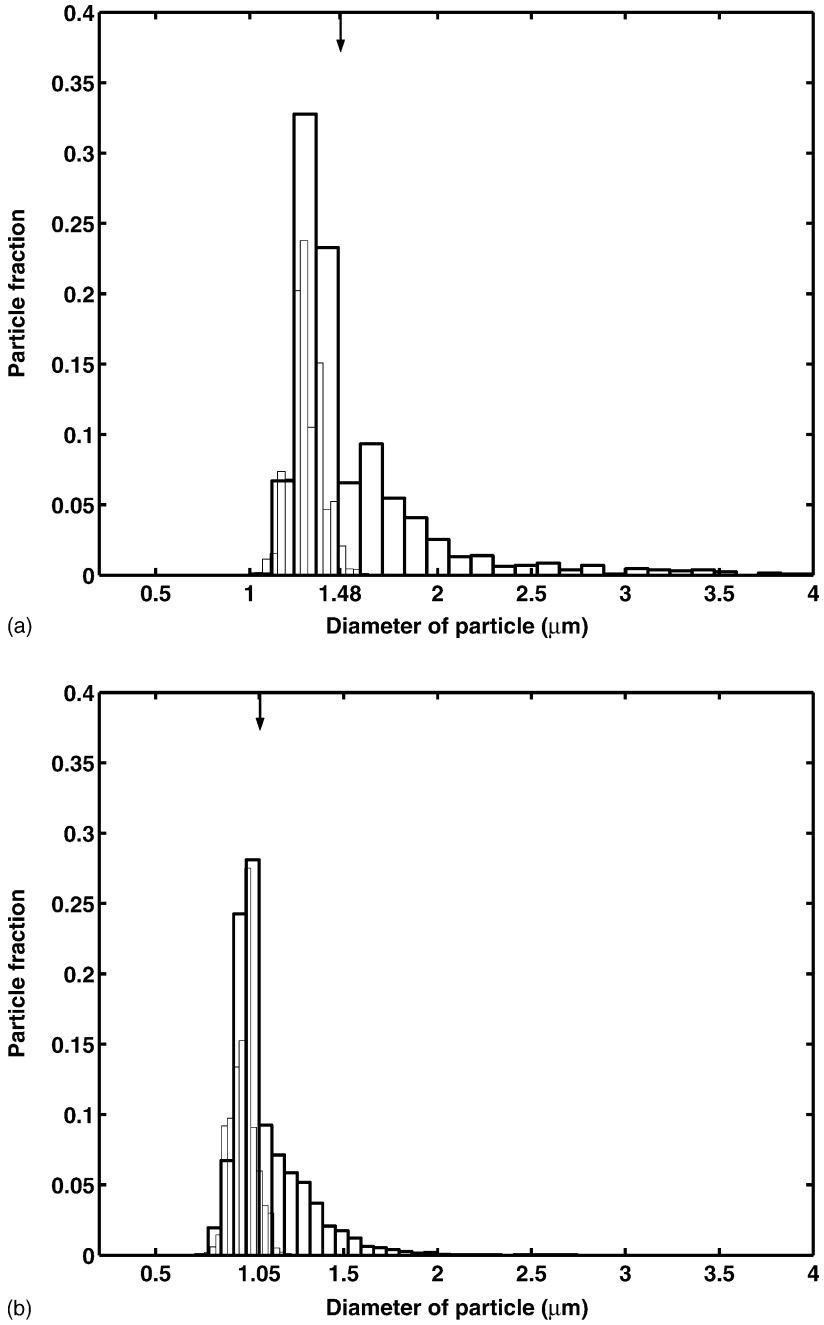

Fig. 9. Size distribution of particles within a control volume before (thin line) and after (thick line) collision. The corresponding laser remelting speeds are (a) 20 mm/s (b) 13 mm/s and (c) 20 mm/s. Average sizes are indicated by the arrows.

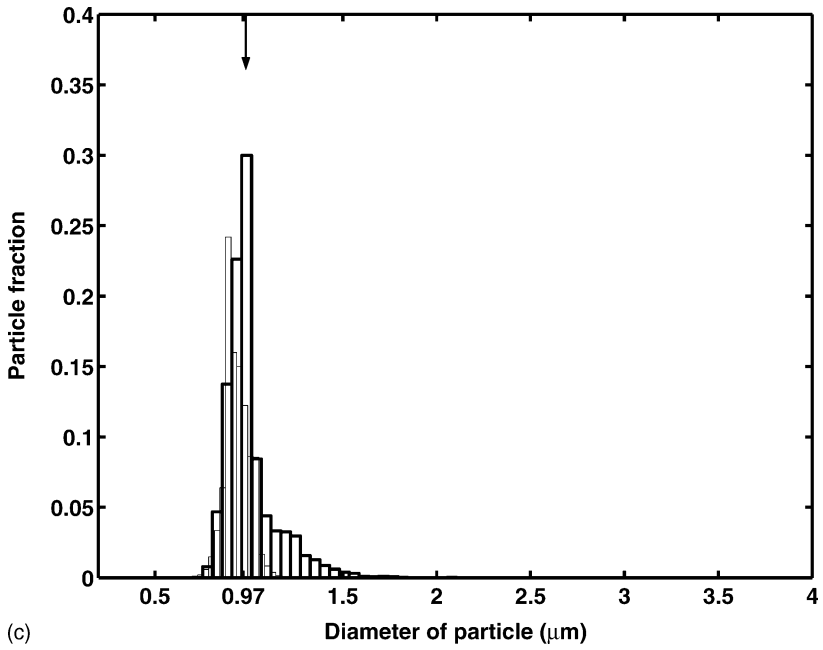

Fig. 9. (*Continued*).

suggest that the simple collision model presented here needs to be improved to obtain a quantitative match for the cases involving lower cooling rates.

6. Conclusions

A distribution of fine bismuth particles in aluminium matrix is achieved by remelting of laser surface alloyed hyper-monotectic alloy. Size distributions of the bismuth particles for alloys remelted at the three different scanning speeds show that higher scan speeds lead to finer bismuth particle size distributions. A two stage computational model that integrates heat and fluid flow as well as phase separation is developed to estimate the size distribution of bismuth particles during laser remelting. The size distribution of bismuth particles is calculated taking simultaneous nucleation and growth by diffusion followed by convection driven coalescence of particles in to account. The agreement between computed and experimental size distributions stresses the importance of convection in the evolution of final microstructure.

Acknowledgements

The authors thank the Chairman, Supercomputing Education and Research Center, Indian Institute of Science for the computational facilities. This work derives support from the Volkswagen Foundation and Department of Science and Technology, Government of India. The authors also thank Prof. S. Ranganathan and Prof. V. Jayaram for fruitful discussions.

References

[1] K. Lepper, M. James, J. Chashechkina, D.A. Rigney, Wear 203–204 (1997) 46.
[2] A.J. McAlister, Bull. Alloy Phase Diag. 5 (1984) 247.
[3] B. Prinz, A. Romero, L. Ratke, J. Mater. Sci. 30 (1995) 4715.
[4] W.K. Thieringer, L. Ratke, Acta Metall. 35 (1987) 1237.
[5] D. Uffelmann, W. Bender, L. Ratke, B. Feuerbacher, Acta Metall. Mater. 43 (1995) 173.
[6] D. Uffelmann, L. Ratke, B. Fuererbacher, Immiscible liquid metals and organics, in: L. Ratke (Ed.), DGM Informationsgesselshaft mbH, Oberursel, Germany, 1993, p. 251.
[7] G. Phanikumar, K. Chattopadhyay, P. Dutta, Int. J. Num. Meth. Heat Fluid Flow 11 (2001) 156.
[8] P. Mohanraj, S. Sarkar, S. Chakraborty, G. Phanikumar, P. Dutta, K. Chattopadhyay, Int. J. Heat Fluid Flow 23 (2002) 298.
[9] S.V. Patankar, Numerical Heat Transfer and Fluid Flow, second ed., Hemisphere Publications, New York, 1980.
[10] L. Granasy, L. Ratke, Scripta Metall. Mater. 28 (1993) 1329.
[11] J.W. Christian, The Theory of Transformations in Metals and Alloys, second ed., Pergamon Press, Oxford, 1975.
[12] L. Ratke, Private Communication, DLR, Cologne, Germany.
[13] C.V. Thompson, F. Spaepen, Acta Metall. 31 (1983) 2021.
[14] F. Falk, Immiscible liquid metals and organics, in: L. Ratke (Ed.), DGM Informationsgesselshaft mbH, Oberursel, Germany, 1993, p. 93.
[15] B. Derby, J. Favier, Acta Metall. 31 (1983) 1123.
[16] L. Ratke, S. Diefenbach, Mater. Sci. Eng. R15 (1995) 263.
[17] C. Zener, J. Appl. Phys. 20 (1949) 950.
[18] L. Ratke, W.K. Thieringer, Acta Metall. 33 (1985) 1793.
[19] L. Ratke, C. Beckermann, Acta Mater. 49 (2001) 4041.
[20] L. Ratke, J. Colloids Interf. Sci. 119 (1987) 391.
[21] R.L. Drake, in: G.M. Hidy, J.R. Brock (Eds.), Topics in Aerosol Research, vol. 2, Pergamon, Oxford, 1972, p. 203.
[22] W. Hoyer, I. Kaban, M. Merkwitz, M3.3, in: Proceedings of the Symposium on Phasenumwandlungen in Schmelzen-II, DPG Frühjahrstagungen, Dresden, 24–28 March 2003 (http://www.ifw-dresden.de/imw/akf2003/).